SEASONAL AND REGIONAL VARIABILITY OF STRATOSPHERIC DEHYDRATION

A Thesis

by

AARON JOSEPH CHRISTENBERRY

Submitted to the Office of Graduate Studies of
Texas A&M University
in partial fulfillment of the requirements for the degree of

MASTER OF SCIENCE

May 2012

Major Subject: Atmospheric Sciences

Seasonal and Regional Variability of Stratospheric Dehydration

SEASONAL AND REGIONAL VARIABILITY OF STRATOSPHERIC DEHYDRATION

A Thesis

by

AARON JOSEPH CHRISTENBERRY

Submitted to the Office of Graduate Studies of
Texas A&M University
in partial fulfillment of the requirements for the degree of

MASTER OF SCIENCE

Approved by:

Chair of Committee,	Andrew E. Dessler
Committee Members,	Steven Quiring
	Robert Korty
Head of Department,	Kenneth Bowman

May 2012

Major Subject: Atmospheric Sciences

ABSTRACT

Seasonal and Regional Variability of Stratospheric Dehydration. (May 2012)

Aaron Joseph Christenberry, B.S., University of Oklahoma

Chair of Advisory Committee: Dr. Andrew E. Dessler

We analyze output from a domain-filling forward trajectory model in order to better understand the annual cycle of water vapor entering the stratosphere. To do this, we determine the minimum water vapor saturation mixing ratio along each trajectory (the final dehydration point or FDP) and assume that the parcel carries that much water vapor into the stratosphere. In the annual average, the tropical Western Pacific, equatorial Africa and South America, and Southeast Asia are found to be the locations of the most frequent FDPs. Looking at individual seasons, we find that FDPs in the tropical western Pacific tend to occur in the summer hemisphere, with FDPs over South America and Africa occurring predominantly during the boreal winter. During boreal summer, a dehydration maximum occurs in the Asian monsoon region. In the annual average, FDP maxima occur at 99 and 84 hPa. Looking at individual seasons, we find that FDPs occur at higher altitudes (centered at 84 hPa) during boreal winter and at lower altitudes (99 hPa) during boreal summer. The annual cycle in FDP altitude combines with the annual cycle in tropical tropopause layer temperatures to generate the observed annual variations in water vapor entering the stratosphere.

ACKNOWLEDGMENTS

The research described in this thesis was funded by NASA grant NNX08AR27G to Texas A&M University. Some material from this thesis has been submitted as an article to the *Journal of Geophysical Research*.

I wish to acknowledge Dr. Andrew Dessler, my committee chair, for his instruction, and the committee members Dr. Steven Quiring and Dr. Robert Korty for serving on the committee. I also thank Dr. Mark Schoeberl, who along with Dr. Dessler designed the model used in this study, and Dr. Kenneth Bowman, for writing the IDL book I used as a tutorial. Tao Wang, a fellow graduate student, deserves acknowledgment for helping me with various debugging issues as well as helping me find various datasets I needed for comparison. Credit is also due to the Geosciences IT staff for fixing the various computer problems that, as is typical when dealing with computers, inevitably arose.

I of course wish to acknowledge my family, without whom I would literally not exist and who have provided me with considerable support, both emotional and—yes—financial as well. Friends and acquaintances from home, undergrad, and the Internet have provided a substantial amount of levity and breakups of what I suspect would otherwise be a very monotonous time.

Naturally, I have had many teachers and professors who I feel are deserving of acknowledgment. I'd first like to thank the Irving Independent School District for enabling me to start taking Algebra I in fifth grade rather than waiting until seventh, and

my parents (again) for being able and willing to shuttle me to and from the middle school. Much courtesy is also due my fifth-grade teacher, Mrs. Glass, and my algebra (and, the next year, geometry) teacher, Mrs. Bennett, for enabling this arrangement—not to mention the administrations of both Townley Elementary and Lamar Middle School. Ultimately, this enabled me to enter college with 59 credit-hours already achieved owing to considerable Advanced Placement testing, though I do not believe this amount is sufficiently high to qualify me for the *Guinness Book of World Records*.

Other teachers I wish to acknowledge are as follows: from elementary school, Mrs. Jackson (Ms. Carlyle at the time), Mrs. Maxwell, and Mrs. Schober; from middle school, Mrs. Vickrey and Mrs. O'Neal; from high school, Mrs. Bradley, Mr. Brock, Mrs. Sargent, and Mrs. Gallemore (and, again, my parents). Professors from my undergraduate tenure at the University of Oklahoma I specifically wish to acknowledge include Dr. Carr, Dr. Fiedler, Dr. Droegemeier, and Dr. Postawko. In addition, I wish to acknowledge Mr. Steven Weiss and Mr. Andrew Dean, who were my advisors for both my undergraduate research in the spring of 2009 and my senior capstone project in 2010.

Finally, I am aware that there are probably people and entities I have missed who deserve acknowledgment; I apologize for failure to include them. Any such person should consider this paragraph as that acknowledgment.

NOMENCLATURE

DJF	December-January-February (boreal winter)
FDP	final dehydration point
H_2O	water vapor
JJA	June-July-August (boreal summer)
MAM	March-April-May (boreal spring)
MERRA	Modern Era Retrospective-Analysis for Research and Applications
MLS	Microwave Limb Sounder
SD2011	*Sherwood and Dessler* [2011] (*Atmospheric Chemistry and Physics* article)
SON	September-October-November (boreal autumn)
TTL	tropical tropopause layer
TWP	tropical Western Pacific
UTLS	upper troposphere/lower stratosphere

TABLE OF CONTENTS

Page

LIST OF FIGURES

FIGURE Page

LIST OF TABLES

1. INTRODUCTION

1.1. Motivation

The role of water vapor (H_2O) in the stratosphere is one of particular importance to climate study. Increases in stratospheric water vapor have a warming effect on the troposphere and a cooling effect on the stratosphere [*Rind and Lonergan,* 1995; *Forster and Shine*, 1999]. Anomalies in stratospheric temperature, in turn, affect the Arctic Oscillation [*Baldwin and Dunkerton*, 1999; *Thompson and Wallace,* 2000] and the teleconnections between the tropospheric El Niño-Southern Oscillation and the North Atlantic–European region [*Cagnazzo and Manzini,* 2009]. Solomon et al. [2010] suggest that the stratospheric H_2O concentration influences the rate of global temperature change. Therefore, understanding the mechanisms by which and locations at which H_2O enters the stratosphere are necessary in order to fully understand the climate system.

1.2. Stratospheric Entry

During his seminal study on stratospheric circulation, *Brewer* [1949] observed that the water vapor mixing ratio, as measured by the frost point, of the stratosphere over the temperate latitudes of southern England was significantly lower than the temperature at the local tropopause would have yielded had the air ascended from the ground directly

---

This thesis follows the style of the *Journal of Geophysical Research*.

beneath the measurement site. From this he inferred the existence of a global stratospheric circulation whereby air predominantly ascends to the stratosphere in the tropics, where tropopause temperatures are coldest. As parcels pass through this cold air, the saturation vapor pressure decreases; when it becomes lower than the parcel's actual vapor pressure, the parcel reaches supersaturation and dehydrates via condensation or deposition. The dehydrated air is then advected poleward in the stratosphere, ultimately descending to the troposphere in the mid-latitude and polar regions. These findings were corroborated by *Dobson* [1956], and the circulation became known as the Brewer-Dobson circulation.

By the 1970s and 1980s, the prevailing interpretation of the Brewer-Dobson paradigm was one of essentially zonally uniform lifting through the tropical tropopause [e.g. *Robinson,* 1980, and references therein]. One challenge encountered by researchers was the fact that even the low zonal-mean temperatures typical of the tropical tropopause are, in most cases, too high. *Ellsaesser* [1983] described this situation in detail, explaining that a 193-K, 100-hPa tropopause should yield H_2O concentrations of 3.4 parts per million by mass [5.6 parts per million by volume (ppmv)], a considerably higher value than observed. The phenomenon of stratospheric air over points in the tropics having an H_2O concentration lower than the local tropopause temperature would suggest was observed in Brazil by *Kley et al.* [1979], who proposed that the air must have dehydrated elsewhere, and by *Jones et al.* [1986].

To explain this discrepancy, *Newell and Gould-Stewart* [1981] proposed the idea of a "stratospheric fountain" in the tropical Western Pacific (TWP) near Indonesia.

They found that this region, during boreal winter (December–February or DJF), has the lowest tropopause temperatures overall, a finding which is corroborated by the studies of *Simmons et al.* [1999], *Highwood and Hoskins* [1998], and *Randel et al.* [2003, 2004]. *Sherwood* [2000] would later discover that the tropopause region over the TWP area in fact exhibits net *downward* motion, weakening the "stratospheric fountain" theory and prompting *Holton and Gettelman* [2001] to rename this area the "cold trap." However, a trajectory analysis by *Hatsushika and Yamazaki* [2003] suggests that the circulation in the TWP TTL is more complex than simple downward motion, and does include areas of ascent.

Two potential mechanisms by which air dehydrates to the low observed H_2O concentrations are commonly referenced. The first entails dehydration by convective overshooting. *Danielsen* [1982] refers to the large anvils of tropical convective clouds as a "dehydration engine," and *Sherwood* [2000] explains that they could be a source not only of dry air but also of cold air. *Sherwood and Dessler* [2000, 2001] present the idea of a "tropical tropopause layer" (TTL), possessing both tropospheric and stratospheric characteristics and extending from approximately 150 hPa to 70 hPa, into which convection overshoots. The existence of such a TTL is now widely accepted, and the properties of the TTL are described in detail by *Fueglistaler et al.* [2009]. Convection can also contribute to dehydration through buoyancy waves [*Potter and Holton*, 1995].

The alternate theory, gradual ascent, also employs the TTL. *Holton and Gettelman* [2001] argued that the large vertical extent of the TTL allowed for considerable horizontal advection of parcels between the time of being uplifted into the

TTL and the time of dehydration and entry into the stratosphere proper. In other words, the "cold trap" of the TWP does not need to be a source of upward motion in order to contribute to dehydration; parcels need only travel horizontally through it, entering the stratosphere proper elsewhere. Additionally, *Jensen et al.* [1996] argued that gravity waves not associated with convection could allow for dehydration in this manner.

Several recent studies suggest that gradual ascent cannot by itself be responsible for stratospheric water vapor. *Moyer et al.* [1996] and *Kuang et al.* [2003] find that the concentration of deuterium in stratospheric water vapor is higher than would be expected through gradual ascent alone. In addition, *Potter and Holton's* [1995] model suggests that buoyancy waves would allow for dehydration to occur at a distance from convection. On the other hand, the model runs of *Gettelman et al.* [2002] and *Jensen and Pfister* [2004] suggest that horizontal advection of air *can* dehydrate air to sufficiently low H_2O concentrations. *Jensen and Pfister*'s study yields H_2O concentrations too *low*, and suggests that convective *moistening* may contribute to the *higher* needed concentrations (by hydrating unsaturated parcels to their saturation mixing ratio [e.g. *Dessler and Sherwood,* 2004]).

Currently, the understanding is that dehydration is a function of both convective and gradual ascent [*Clark et al.,* 2001; *Rosenlof*, 2003]. The relative importance of their roles, however, is still a matter for debate. Additionally, convection is not a constant even in the tropics; as such, the relative importance of their roles may change as a function of space and time.

1.3. Seasonal and Regional Variability

The concentration of stratospheric H_2O is generally quite low and varies both with location and with time. *Mastenbrook* [1971] observed the mixing ratio in the lower stratosphere over Washington, D.C. to be in the range of 1–4 ppm by mass, (approximately 2–7 ppmv), with the amplitude of the seasonal variability ranging from 0.2–0.5 ppm (0.3–0.8 ppmv) depending on altitude. *Harries* [1976] found the mixing ratio range to be from 0.5–5 ppm by mass (0.8–8 ppmv).

The dominant mode of seasonal variability in stratospheric H_2O is the so-called "tape recorder" [*Mote et al.,* 1996]. At the tropopause in late boreal summer, water vapor concentration is at a maximum (the moist phase); in late boreal winter it is at a minimum (the dry phase). These maxima and minima increase in height as a function of time, such that when water vapor concentration is plotted as a function of time and height, the result is a series of diagonal bands resembling the magnetic tape of a tape recorder (see e.g. Fig. 4a in *Mote et al.* [1996], Fig. 7c in *Schoeberl and Dessler* [2011]). Similar tape recorder effects have been observed in carbon dioxide [*Andrews et al*., 1999], carbon monoxide [*Schoeberl et al.,* 2006, *Randel et al.,* 2007], and hydrogen cyanide [*Randel et al.,* 2010, *Pommrich et al.*, 2010], but the tape recorder in water vapor is the most closely correlated to TTL temperature.

The mean tropopause temperature experiences a seasonal oscillation, with an annual global minimum in DJF and a maximum in JJA (*Scaife et al.* 2000). Using Global Positioning System Meteorology (GPS/MET) data, *Randel et al.* [2004] observe a seasonal cycle in the TTL possessing, at some locations and altitudes, an amplitude of

as high as 8 K. The seasonal cycle is not, however, zonally uniform, as best seen in their Figure 5, complicating understanding of the tape recorder. *Vömel et al.* [2002], after analyzing the vertical profiles of water vapor and ozone at several points in the tropics during different times of year, also came to the conclusion that regional and seasonal differences matter.

Because the TTL is not uniform in either space or time, it follows that an understanding of the regional and seasonal variations in parcel dehydration and contribution to the tape recorder and H_2O concentration of the stratosphere is necessary. In other words, the locations at which parcels dehydrate and the differences in these locations by season must be determined.

An obvious first candidate is, of course, the TWP. Its possession during DJF of the lowest tropopause temperatures overall were, after all, what led *Newell and Gould-Stewart* [1981] to postulate this area as a "stratospheric fountain" in the first place. The cold-point tropopause over the TWP exhibits both a seasonal water vapor oscillation and a seasonal altitude oscillation from 16 km in boreal summer and early boreal autumn to 17 km in boreal winter and early spring as measured by *Reid and Gage* [1996] on the island of Truk (7.5°N, 151.8°E). Using a scale height of 7 km [*Holton et al.,* 1995], these 16-km and 17-km heights equate to pressures of 103 hPa and 89 hPa, respectively. *Vömel et al.* [2002]'s H_2O profiles indicate extremely low March water vapor concentrations in the TWP and tropical central Pacific in the altitude vicinity of the tropopause relative to Brazil and the eastern Pacific, and *Fueglistaler et al.* [2005] find the TWP to be an area of significant dehydration.

The Asian monsoon, owing to its status as a large-scale seasonal convective event and its proximity to the TWP, also is an area of particular interest. *Dunkerton* [1995] finds evidence of a strong southward component to the circulation at upper troposphere/lower stratosphere (UTLS) levels in the region ranging from China to the central Pacific, and states that parcels in this circulation exhibit "significant penetration into the stratosphere." *Park et al.* [2007]'s study finds the area over China and the northwestern Pacific to have significant upward motion at tropopause altitudes, with the vertical velocity highest in the 10–20°N latitude range (refer to their Fig. 12). Near-tropopause H_2O concentrations in this area are generally relatively high [*Randel et al., 2001*; *Gettelman et al.,* 2004; *Dessler and Sherwood*, 2004] and have been found to be a significant source of H_2O in boreal summer [*Fueglistaler et al.,* 2005; *Wright et al.,* 2011].

Additionally, trajectory analyses done by *Gettelman et al.* [2004], *Fueglistaler et al.* [2004], and *Wright et al.* [2011], global climate model analyses done by *Bannister et al.* [2004], and Aura Microwave Limb Sounder (MLS) and Tropical Rainfall Measuring Mission (TRMM) observations made by *Fu et al.* [2006] suggest that advection around the monsoon anticyclone can result in H_2O bypassing the tropical tropopause altogether. Such a bypass entails air entering the stratosphere via a warmer subtropical or extratropical tropopause in the Northern Hemisphere and then is brought southward by the monsoon circulation into the tropical stratosphere. *Wright et al.* [2011] and *Fu et al.* [2006] focus particularly on the Tibetan plateau region, suggesting that this portion of the monsoon in particular may be the most likely to bypass the tropopause.

1.4. Thesis Goals and Structure

The goal of this thesis, therefore, is to determine and quantify the contribution of world regions to dehydration and stratospheric H_2O, and to determine the seasonal variations in these contributions, including the contribution of each region to the overall annual cycle of water vapor (i.e., the "tape recorder" effect). Section 2 describes the model and data used to find these contributions. Section 3 details the methods used to calculate and determine the results; the results themselves are presented and discussed in Section 4. Section 5 presents our conclusions.

2. MODEL

The goal of this study is to analyze locations of dehydration, and in particular the point at which a parcel reached its lowest H_2O concentration, referred to as the final dehydration point (FDP). The occasion of a parcel reaching its FDP is referred to as an "FDP event." As parcels can be horizontally advected and encounter multiple dehydration points within the TTL before entering the stratosphere [*Holton and Gettelman,* 2001], a Lagrangian trajectory model is more helpful for TTL dehydration analysis than an Eulerian model.

The particular model used for this study is the domain-filling forward trajectory model described in great detail in *Schoeberl and Dessler* [2011, hereafter SD2011]. Briefly, the model uses the Bowman trajectory code [*Bowman,* 1993; *Bowman and Carrie,* 2002] driven by horizontal winds and diabatic heating rates from the Modern Era Retrospective-Analysis for Research and Applications (MERRA) [*Rienecker et al.,* 2011]. Diabatic transport means that potential temperature θ is used for the vertical coordinate and that vertical (i.e. non-isentropic) motion is determined by the diabatic heating rate [SD2011]. The model can also be run using a kinematic transport scheme (vertical coordinate is pressure p; motion across isobars is determined by $\omega=dp/dt$); however, as explained by *Liu et al.* [2010] and SD2011, the kinematic scheme is too dispersive.

The particular model run used in this study is the equivalent of SD2011's "D100" run, which does not take supersaturation and gravity waves into account but which

nevertheless agrees well with Aura Microwave Limb Sounder (MLS) data [SD2011, see their Table 1]. Methane oxidation, convective moistening and re-evaporating condensate, which have a moistening effect [e.g. *Dessler et al.,* 1994; *Mote et al.,* 1996; *Dessler et al.,* 2007; *Liu et al.,* 2010], are also excluded, giving the model a somewhat dry bias.

The grid used in this study has been modified somewhat from SD2011. Each run of the model initializes a grid of 1350 parcels each day over a one-year period, and advects the parcels until the end of the tenth year following initialization (i.e. parcels initialized in 1995 are advected until the end of 2005). In this study we use runs with initialization years of 1993–2010. Though MERRA data are available starting from 1979, we utilize the 1993 start date to minimize contamination by climatologically abnormal results arising from the Pinatubo eruption in June 1991. Parcels are initialized on the 365-K θ surface, which is above the zero net radiative heating level but typically below the tropical tropopause (~375–380 K). The initial grid is an equal area grid that spans all longitudes and runs from 60°S to 60°N, with a resolution of 3-5° latitude and 8° longitude. Parcels that end a day below the 250 hPa pressure level are assumed to have re-entered the troposphere and are removed from the model; the same applies for parcels that ascend beyond 1800 K—these are assumed to have entered the mesosphere and are removed. We use the simplest possible microphysical parameterization to estimate the water vapor along the trajectory: when the relative humidity (RH) of the parcel exceeds 100%, excess water vapor is removed so as to return the RH to 100%. SD2011 describes the model in further detail.

The model was set to produce file output detailing the position and composition of each parcel on the 1st, 8th, 15th, 22nd, and 29th of each month. This file output includes, among other parameters, a unique ID tag for each parcel in the run, the H_2O concentration of the parcel at the time of output (which, because condensate re-evaporation and methane oxidation are excluded, is effectively equivalent to the concentration at the previous point of dehydration); the date of the previous dehydration event (i.e. the dehydration event that occurred most recently relative to the time of output); and the latitude, longitude, temperature, and pressure of the parcel at the time of the previous dehydration event.

Water vapor data from the Aura Microwave Limb Sounder (MLS) was used to compare our model results with observations. MLS water vapor observations are validated by *Livesey et al.* [2005] and have a vertical resolution of 2-3 km and UTLS-level accuracy of 5-7% (0.3 ppmv) [*Lambert et al.,* 2007; *Read et al.,* 2007]. Using Halogen Occultation Experiment (HALOE) data for comparison was considered; however, HALOE's accuracy peaks in the altitude range of 1–10 hPa, well above the UTLS level [*Harries et al.,* 1996, see in particular their Table 1]. Furthermore, SD2011 used MLS data; using it here would thus provide consistency that using HALOE data would not.

3. METHODS

3.1. Determining the FDP

Because the model is necessarily unaware of the future behavior of the parcels at the time it outputs its results to disk, the "final dehydration data" given in the results are in fact the data for the *most recent* dehydration event. To minimize the probability that the dehydration event reported by the model is *not* the final tropical dehydration event, we process the data backward using the method described below.

We first look at 22 December of the final available year of the particular run (2010 or the initialization year plus 10, whichever is earlier); this date is the observation date. The 22nd of the month is used because it is approximately halfway between the middle of the month (simulating monthly averages) and the end of the month (maximizing data availability), and the last output date before the end of the month that all months can be assured to have (since February typically has only 28 days). We treat as valid for analysis all parcels that (1) were above 90 hPa at the time of observation, (2) had their most recent dehydration event at least 180 days prior to observation, and (3) had their most recent dehydration event at least 2 days following initialization. Restricting our analysis to parcels above 90 hPa at observation ensures that we are only concerning ourselves with parcels that have ascended considerably higher than the initialization point. Excluding dehydration events that occur less than 180 days before observation increases the probability that the most recent dehydration event is, in fact, the *final* dehydration event. Finally, requiring the dehydration event to be at least 2 days

following initialization decreases the number of parcels that are instantiated above the cold point from consideration. If all three parameters are met, the H_2O concentration, temperature, and location of these parcels as of their previous dehydration are taken as the FDP H_2O, temperature, and location parameters and are stored as such under the parcel ID.

Though most studies of the tape recorder focus on activity near the equator (*Mote et al.* [1996], for instance, used ±12° latitude; SD2011 used ±1° latitude), we find that broadening the field to include the subtropics does not appreciably diminish the annual water vapor cycle (Table 1). In addition, we find that no appreciable difference arises from using 180 days before the observation date as a cutoff relative to other choices (not shown). Excluding parcels whose most recent dehydration occurs less than 2 days after initialization, however, *does* make a significant difference, removing parcels that are moister than they should be owing to their initialization above the cold point (Table 2).

After determining the FDP parameters for parcels available on 22 December of the final year, we do the same for each preceding month, changing the observation date to 22 November of the final year, then 22 October, then 22 September, and so forth until we reach the beginning of the run. FDP parameters are determined for all parcel IDs in the run that have not had FDP parameters determined in a later (i.e., previously processed) month. Once each run has been fully processed, we proceed to the next run and apply the same procedure. Figure 1 depicts this process as a flowchart.

3.2. Regional Binning and Unit Normalization

Latitude-longitude regional analyses were conducted by dividing the world into 2° latitude by 5° longitude bins, spanning the entire globe meridionally and the range from 40°S to 40°N zonally; pressure analyses were conducted by dividing the altitude range from 60 hPa to 120 hPa into 2-hPa bins. These bins represent the location or altitude at which the parcels underwent their FDP event. This resolution was observed to be fine enough to capture significant small-scale detail, while being coarse enough that instances of zero data points within the bin are rare.

Parcel FDP event distribution analyses entail the counting of parcels that underwent their FDP event within a certain region or at a certain altitude. Because the number of parcels instantiated on the grid is essentially arbitrary (changing this number only changes the mass of air considered as each parcel), to ensure that our results are applicable to any instantiation grid, we normalize the parcel counts by the overall total number of parcels and further divide by the bin size (e.g. 5° longitude by 2° latitude). This yields units of "percent per degree latitude per degree longitude" or "percent per hectopascal," which is not dependent on how many parcels were used.

One disadvantage of using regions of equal latitudinal and longitudinal extent in binning rather than equal-area bins as the model initializes the parcels is that regions at different latitudes are of different areas—the earth's circumference is greater at the equator than at, say, 30°N. While this does not pose a problem for datasets that do not represent counts, it means that a count of parcels does not technically equate to mass. However, because this study focuses on the tropics, where the difference between equal-

area and latitude-longitude bins is not substantial, parcel count can be treated as approximately equivalent to mass.

3.3. Pseudo-Fluxes

In a Lagrangian trajectory framework, the number of parcels within a region at a specific point in time is analogous, though not equivalent, to the mass flux through that region at that point in time. In particular, the number of FDP events within a region is analogous to the mass flux crossing the FDP point within that region.

The water vapor flux is the mass of water vapor, and can be calculated by multiplying the mass of a given amount of air by the percentage by mass of water vapor in it. For our framework, this is equivalent to multiplying the H_2O concentration by the number of FDP events, as shown in the below equation:

$$F_p(p,t) = N(p,t)\,q(p,t) \tag{1}$$

where F_P is the flux proxy (pseudo-flux), p pressure, t time (in months), N the number of FDP events per pressure unit per month, and q the mean FDP saturation H_2O (which is analogous to the FDP temperature). Because water vapor is given in parts per million by *volume* rather than by mass, and because, as previously mentioned, we are using latitude-longitude regions rather than equal-area regions to conduct the analyses, the product of the mean H_2O concentration and number of FDP events is not a true flux but a pseudo-flux.

Looking at N or q as a function of height only gives us the vertical profile of FDP events or FDP saturation H_2O, which changes over time. To determine their effect, we

decompose the flux by forcing one of these to be held at its average annual value while we vary the other. In reality, *N* and *q* are not independent of each other, but we can separate them in our model to estimate their individual impact. In other words, we force the vertical profile of FDP events to remain constant at its annual mean for each height, but allow the vertical profile of water vapor to vary, i.e.,

$$\frac{\partial}{\partial t}\bar{N}(p,t) = 0 \;\therefore\; \bar{N}(p,t) = \bar{N}(p) \tag{2a}$$

$$\bar{N}(p) = \frac{1}{12}\sum_{t=1}^{12} N(p,t) \tag{2b}$$

where $\bar{N}(p)$ is the annual mean FDP event count for each pressure level *p*. We do the same for the water vapor profile, holding it (and thus the vertical temperature profile) constant; i.e.,

$$\frac{\partial}{\partial t}\bar{q}(p,t) = 0 \;\therefore\; \bar{q}(p,t) = \bar{q}(p) \tag{3a}$$

$$\bar{q}(p) = \frac{1}{12}\sum_{t=1}^{12} q(p,t) \tag{3b}$$

where $\bar{q}(p)$ is the annual mean H_2O concentration for each pressure level *p*.

We then multiply these mean values by the actual values of the other parameter to get a pseudo-flux, and divide by whichever monthly parcel count (actual or average) was utilized. This gives us what *would* be the mean monthly water vapor concentration if the vertical profile being held constant was actually constant, i.e.,

$$q_{\bar{N}}(t) = \frac{\sum_p (N * \bar{q})}{\bar{N}} \tag{4a}$$

$$q_{\bar{q}}(t) = \frac{\sum_p (N * \bar{q})}{\sum_p N} \tag{4b}$$

where $q_{\bar{N}}$ is the monthly mean FDP point H_2O holding the vertical FDP profile constant and $q_{\bar{q}}$ is the monthly mean FDP point H_2O holding the vertical H_2O profile constant.

4. RESULTS

4.1. Tape Recorder Test

To test whether the model can reproduce the seasonal cycle of the tape recorder, in Figure 2 we plot the average H_2O concentration emerging from the FDP event as a function of the month in which the parcel was dehydrated.

A clear annual cycle is evident, with a maximum in boreal summer and a minimum in boreal winter, as would be expected in the tape recorder. For comparison, also plotted in Figure 2 is the average water vapor concentration at 82 hPa (near the top of the TTL) during each month measured by MLS. Though MLS data is available at altitudes below 82 hPa, we choose this level to show more readily the persistence of the tape recorder with height. The MLS data is offset by 1.5 months to account for lag between the occurrence of the FDP events and the time at which their influence reaches 82 hPa.

Apart from the lag, the main discrepancy between the MLS data and model output is the dry bias of about 0.3 ppmv evident in the model output. This was expected by our exclusion of convective moistening and similar processes that increase the water vapor content of the stratosphere [SD2011]. However, the amplitude of the seasonal cycle in both is approximately 2.2–2.4 ppmv, which gives us confidence in our analysis of the FDP statistics and that, adjusted for the dry bias, we can treat this as an accurate result. This calculation agrees well with previous work that has shown the seasonal cycle can be accurately simulated by this type of model [e.g., *Fueglistaler et al.*, 2005].

4.2. Annual Dehydration Statistics

Figure 3 shows the latitude-longitude distribution of FDP events in the model. The predominant maxima are at 10°N and 10°S over the TWP. Smaller maxima are located over South America and Africa, regions which also experience frequent deep convection. The average saturation H_2O concentration associated with the FDP events is plotted in Figure 4. The H_2O concentration minima are approximately collocated with the FDP maxima. The existence of the maximum around Australia, however, is questionable and a possible bias of the MERRA reanalysis data; a paper in preparation will investigate this bias in detail (Schoeberl et al., in preparation).

The annual average MERRA reanalysis 100 hPa temperature is contoured on Figures 3 and 4. One can clearly see that the areas of maximum final dehydration frequency also possess the coldest annual mean temperatures and are therefore H_2O concentration minima. In general, global dehydration is very nearly bounded by the 194-K isotherm, and the regions with the *most* frequent dehydration have annual mean 100-hPa temperatures below 192 K. The temperature maximum off the equatorial east African coast is associated with little dehydration, consistent with expectation.

Southeast Asia provides a notable exception to the general rule of "low temperatures yield low water vapor." FDP saturation H_2O there is higher than the temperature suggests it should be, implying the presence of a significant localized seasonal variation, a cold-point bypass mechanism, or both. This further underscores the significance of the Asian monsoon region in determining stratospheric water vapor

Figure 5 shows the vertical distribution of FDP events (solid line). Dehydration occurs almost exclusively between 70 and 110 hPa, and exhibits a bimodal distribution with distinct maxima at 84 hPa and 99 hPa. The pressure levels of the maxima correspond to 17 and 16 km, the altitudes of the tropopause height cycle observed by *Reid and Gage* [1996], providing evidence in favor of a connection between this seasonal height cycle and the bimodal dehydration distribution.

The thin dashed line in Figure 5 represents the average H_2O concentration associated with the FDP events, which decreases with height up until approximately the 84 hPa dehydration maximum. Above 84 hPa, the saturation H_2O concentration increases, suggesting that parcels whose FDP events are above this altitude are fully in the stratosphere, with temperature increasing with height, when they dehydrate. This can be accomplished only by bypassing the tropical cold point and entering the stratosphere in the subtropics or extratropics or by being uplifted through extremely vigorous convection to unusually high altitudes.

4.3. Seasonal Dehydration Statistics

4.3.1. Latitude–longitude

Figure 6 shows the latitude-longitude FDP distribution in each meteorological season; month-by month statistics of a variety of parameters (parcel count, H_2O, temperature, etc.) are available in Table 3. Figure 6 is similar to Figure 9 of SD2011, which also shows FDP event distribution, but we include the MERRA 100-hPa average temperature distribution for each season in analogy with Figure 3. The plots are of the

percentage of FDP events that occurred during that season relative to the total of FDP events that occurred anytime in the year, so that the sum of the FDP events in Figure 6 equals Figure 3.

While the FDP event frequency is elevated throughout the year in the TWP, this figure clearly shows that the TWP dual maxima seen at 10°N and 10°S in Figure 3 are two different phases of a seasonal cycle. FDP events over South America and Africa also exhibit a strong seasonal cycle, being most prominent in boreal winter (DJF) and vanishing entirely during boreal summer (JJA). Overall, FDP events tend to occur preferentially in the hemisphere experiencing summer. One can also see in Figure 6 that FDP events themselves exhibit a seasonal cycle. Quantitatively, 31.1% of all events in the observation period occurred in DJF, whereas only 22.1% occurred in SON, the minimum. MAM and JJA experienced 24.4% and 22.5%, respectively (see Table 3 for month-by-month statistics using the parcel counts from our gridding method). We reiterate that the existence of the DJF maximum over Australia may be attributable to a MERRA bias.

4.3.2. Vertical

Figure 7 displays the time series of the vertical distribution of FDP events. The month of the FDP event is on the abscissa and the pressure on the ordinate. This figure clearly shows that the bimodal distribution seen in Figure 5 is attributable to a seasonal cycle, with distinct boreal winter and boreal summer modes. The boreal winter mode is associated with dehydration in the 80–90 hPa pressure range (peaking at 84 hPa, cf. Fig.

3), and persists from early October through early May. The boreal summer mode is associated with dehydration in the 90–105 hPa pressure range (peaking at 99 hPa) and persists from early April through the end of September. The small maximum around 73 hPa is visible only in December–January, ruling out this maximum being attributable to the Asian monsoon bypass mechanism postulated by *Bannister et al.* [2004] and others; one possibility is that it is due to unusually deep convection reaching well above the cold point. It is clear, though, that this 73-hPa maximum is insignificant and only of marginal interest.

From Figure 7 we can clearly see that during MAM, the winter mode remains active, albeit weakening, even as the summer mode becomes active. This phenomenon does not occur during SON, where the summer mode ceases at approximately the same time (late September–early October) as the winter mode becomes active. The activity of both the summer and winter modes during MAM results in a higher overall frequency of FDP events during that season, particularly as lower-altitude dehydration events actually maximize in May–June (Table 3).

The saturation H_2O associated with the FDP events is plotted in Figure 8. The effects of the seasonal cycle in TTL temperature on H_2O can be clearly seen at all altitudes: parcels dehydrating during DJF at any altitude are colder and therefore drier than parcels at the same altitude dehydrating during JJA. Above approximately 95 hPa, the water vapor cycle does not perfectly match the meteorological seasons but is shifted forward a month; this asymmetry is driven by the TTL being warmer in SON than in MAM. The monsoon, whose peak is in mid-May through mid-August depending on

location [*Wang and LinHo,* 2002], is the likely reason for the earlier water vapor maximum beneath 95 hPa. Similarly, the significant spike in H_2O concentration during August–October between 65–75 hPa is likely attributable to the handful of parcels that bypassed the cold point by being advected around the Asian monsoon anticyclone (hence the later dehydration date) or by being uplifted by unusually vigorous convection. These instances are rare but occur in areas with little dehydration, and thus have a large effect on the local dehydration H_2O concentration.

Apart from these discrepancies, however, the general profile of water vapor in the stratosphere is the same irrespective of time of year. During any month of the year, parcels dehydrating at approximately 80–90 hPa, and especially between 83–85 hPa, have the lowest water vapor concentrations (and thus temperatures) relative to other levels in the same month.

These results imply that the annual cycle of water entering the stratosphere is driven by two factors: changes in the altitude of dehydration and changes in the temperature of the TTL. The moist phase of the annual cycle maximizes in boreal summer to early autumn, when the TTL as a whole is warmer and dehydration is occurring primarily at the lower and warmer summertime maximum. Both of these tend to increase the amount of water carried into the stratosphere. The dry phase occurs during DJF, when the TTL as a whole is coldest and dehydration is occurring at the higher, cooler wintertime maximum. This allows a larger annual oscillation of H_2O concentrations than would be expected due to 100-hPa temperature differences alone [e.g. *Frederick and Douglass,* 1983; *Mote et al.,* 1995].

4.3.3. Zonally averaged

To compare the vertical plots with the latitude-longitude seasonal variation, we recreate Figures 7 and 8 but plot latitude on the ordinate rather than pressure (Fig. 9, 10). Figure 9 thus displays the frequency of FDP events as a function of latitude and month, with units of percent per degree latitude (zonally averaging all longitudes together. The actual counts of parcels using our gridding method are given in Table 4). Figure 10 displays the average H_2O concentration of each FDP event.

Figure 9 clearly shows a generally smooth transition in dehydration events from the SH in November–January to the NH in April–June, followed by a marked cessation in the late boreal summer and early boreal autumn. Though horizontal, the pattern bears a striking resemblance to the tape recorder. The comparative absence of dehydration events is collocated with the water vapor maximum after dehydration both at the latitude and altitude average (Figs. 8, 10).

The difference in land coverage in the southern hemisphere versus the northern hemisphere offers a possible reason for this phenomenon. The water-dominated Southern Hemisphere is more stable climatically owing to water's higher heat capacity relative to land. In austral autumn (boreal spring), the largely-marine surface takes longer to cool down, enhancing upper-level divergence and upwelling into the stratosphere. Conversely, the Northern Hemisphere's land surface heats quickly (particularly in the vicinity of Asia, the largest landmass) in boreal spring. Upwelling into the stratosphere thus begins earlier in the year, and is aided by the monsoon circulation.

Late boreal summer and boreal autumn are associated with the termination of the monsoon, comparatively rapid cooling of the land-dominant Northern Hemisphere, and relatively slow warming of the water-dominant Southern Hemisphere. The summer mode therefore ceases more rapidly than the winter mode can re-form, resulting in a decrease in overall FDP event frequency during these months. Because this also happens during the time of year when TTL temperatures (and thus FDP saturation water vapor mixing ratios) are at their highest, the stratosphere is drier than it otherwise would be, as observed by e.g. *Kley et al.* [1979]. This phenomenon also would explain the presence of overlap in the summer and winter modes during MAM and the comparative absence of both modes during SON—the summer mode starts (or ends) before the winter mode begins

4.4. Relative Importance of Temperature and Height

Decomposing the pseudo-flux using the method described in Section 3.4 allows us to determine the comparative contribution of the vertical profile of TTL temperature vs. FDP frequency. Figure 11a shows the monthly time series of water vapor produced by decomposing the pseudo-flux via the method described in Section 3.4. The solid line is the monthly average time series of saturation mixing ratio from Figure 2; the dashed line is the time series that would occur if the vertical distribution of FDP frequency were fixed at its annual average value (plotted in Fig. 5) but allowing the FDP saturation mixing ratio to vary through time (as plotted in Fig. 8). The dotted line is the time series that would occur if the vertical profile of the TTL temperature, and thus the FDP

saturation mixing ratio, were held constant at its annual average, but allowing the vertical FDP frequency profile to vary in time (as plotted in Fig. 7).

We observe that the dashed line closely parallels the solid line, meaning that the contribution of FDP altitude alone to the annual cycle is small. It is not, however, entirely negligible, as the seasonal cycle in its anomaly relative to the true saturation mixing ratio is oriented opposite to the seasonal cycle in the true saturation mixing ratio (Fig. 11b), meaning that excluding this contributor results in a dampening of the annual cycle (and that including it enhances it). The dotted line, on the other hand, exhibits little seasonal cycle and its anomaly is strongly oriented against the saturation H_2O cycle, meaning that the seasonal cycle of water vapor entering the stratosphere is predominantly determined by the seasonal cycle in TTL temperature—excluding this cycle results in hardly any variation from month to month.

5. CONCLUSIONS

We have used a domain-filling forward trajectory model to investigate the seasonal cycle of dehydration in the TTL. The model has no convective parameterization and dehydration is set to 100% saturation [SD2011]. The model uses MERRA reanalysis and initializes parcels just below the tropopause and advects them until they exit the stratosphere. For each parcel, we have identified the point on its trajectory where it encounters the lowest water vapor saturation mixing ratio, which occurs at the final dehydration point (FDP) and which we refer to as an FDP event. By assembling the statistics of these FDP events, we can gain insight into the mechanisms that control the seasonal cycle of water entering the stratosphere.

In the annual average, we see that FDP events occur preferentially in regions where deep convection also frequently occurs (although we do not parameterize this process). Analyzing the seasonal cycle, we find that FDP events preferentially occur in each season's spring/summer hemisphere. During DJF, parcels dehydrate primarily in the TWP between the equator and 10°S, though this southern hemisphere bias may be unique to the MERRA reanalysis (Schoeberl et al., in preparation). During JJA, parcels dehydrate primarily in the Asian monsoon region. We also see FDP events occurring over equatorial South America and Africa during DJF, but not in JJA. Boreal spring exhibits more frequent dehydration than boreal autumn,

There is also a strong seasonal cycle in altitude: FDP events occur at the highest altitudes during DJF and at the lowest altitudes during JJA. The altitude of the FDP

event affects the dehydration potential of that event; higher altitude events tend to have lower saturation mixing ratios, leading to drier air. Additionally, there is a seasonal cycle in TTL temperatures, with the warmest TTL occurring at the same time as the lowest-altitude FDP events. Both of these tend to allow more water vapor through the TTL and into the stratosphere during JJA, consistent with the annual variation in water vapor that gives rise to the dehydration cycle, but the seasonal cycle in temperature contributes to the annual dehydration cycle's development more than the seasonal cycle in TTL height. The TTL is slightly warmer in SON than in MAM owing in part to the differences in hemispheric land/water ratios and subsequent differential heating, so the moist phase of the annual cycle lasts into SON and the dry phase lasts into MAM.

The dry phase of the annual stratospheric dehydration cycle is therefore driven by a flux of colder, drier air with FDP locations primarily in the TWP. The moist phase is driven by a flux of warmer, moister air with FDP locations primarily in the Asian monsoon and north of Australia. The stratosphere is drier overall than the average TTL temperature would appear to indicate because parcels preferentially avoid entering the stratosphere during the times of year when the water vapor mixing ratio after dehydration is at its highest.

REFERENCES

Andrews, A. E., K. A. Boering, B. C. Daube, S. C. Wofsy, E. J. Hintsa, E. M. Weinstock, and T. P. Bui (1999), Empirical age spectra for the lower tropical stratosphere from in situ observations of CO_2: Implications for stratospheric transport, *J. Geophys. Res.*, 104(D21), 26,581–26,595, doi:10.1029/1999JD900150.

Baldwin, M. P., and T. J. Dunkerton, 1999: Propagation of the Arctic Oscillation from the stratosphere to the troposphere. *J. Geophys. Res.*, 104, 937–940, 946.

Bannister, R. N., A. O'Neill, A. R. Gregory, and K. M. Nissen (2004), The role of the south-east Asian monsoon and other seasonal features in creating the 'tape-recorder' signal in the Unified Model, *Q. J. R. Meteor. Soc.,* 130, 1531–1554, doi:10.1256/qj.03.106.

Bowman, K. P. (1993), Large-scale isentropic mixing properties of the Antarctic polar vortex from analyzed winds, *J. Geophys. Res.,* 98**,** 23,013–23,027.

Bowman, K. P., and G. D. Carrie (2002), The mean-meridional transport circulation of the troposphere in an idealized GCM, *J. Atmos. Sci.,* 59, 1502–1514, doi:10.1175/1520-0469(2002)059<1502:TMMTCO>2.0.CO;2

Brewer, A. W. (1949), Evidence for a world circulation provided by the measurements of helium and water vapour distribution in the stratosphere, *Q. J. R. Meteor. Soc.,* 75, 351–363.

Cagnazzo, C., and E. Manzini, 2009: Impact of the stratosphere on the winter tropospheric teleconnections between ENSO and the North Atlantic and European region. *J. Climate*, 22, 1223–1238.

Clark, H. L., A. Billingham, R. S. Harwood, and H. C. Pumphrey, 2001: Water vapor in the tropical lower stratosphere during the driest phase of the "tape recorder". *J. Geophys. Res.,* 106(D19)**,** 22 695–22 705.

Danielsen, E. F. (1982), A dehydration mechanism for the stratosphere, *Geophys. Res. Lett.*, 9(6), 605–608, doi:10.1029/GL009i006p00605.

Dessler, A. E., E. M. Weinstock, E. J. Hintsa, J. G. Anderson, C. R. Webster, R. D. May, J. W. Elkins, and G. S. Dutton (1994), An examination of the total hydrogen budget of the lower stratosphere, *Geophys. Res. Lett.*, 21(23), 2563–2566, doi:10.1029/94GL02283.

Dessler, A. E., and S. C. Sherwood (2004), Effect of convection on the summertime extratropical lower stratosphere, *J. Geophys. Res.*, 109, D23301, doi:10.1029/2004JD005209.

Dobson, G. M. B. (1956), Origin and distribution of the polyatomic molecules in the atmosphere, *Proc. Roy. Soc. London,* 236, 187–193.

Dunkerton, T. J. (1995), Evidence of meridional motion in the summer lower stratosphere adjacent to monsoon regions, *J. Geophys. Res.*, 100(D8), 16,675–16,688, doi:10.1029/95JD01263.

Ellsaesser, H. W. (1983), Stratospheric water vapor, *J. Geophys. Res.*, 88(C6), 3897–3906, doi:10.1029/JC088iC06p03897.

de F. Forster, P. M., and K. P. Shine (1999), Stratospheric water vapour changes as a possible contributor to observed stratospheric cooling, *Geophys. Res. Lett.*, 26(21), 3309–3312, doi:10.1029/1999GL010487.

Frederick, J.E., and A.R. Douglass (1983), Atmospheric temperatures near the tropical tropopause: Temporal variations, zonal asymmetry and implications for stratospheric water vapor, *Mon. Wea. Rev.*, 111, 1397-1403, doi:10.1175/1520-0493(1983)111<1397:ATNTTT>2.0.CO;2

Fu, R., Y. Hu, J. S. Wright, J. H. Jiang, R. E. Dickinson, et al. (2006), Short circuit of water vapor and polluted air to the global stratosphere by convective transport over the Tibetan Plateau, *Proc. Nat. Acad. Sci.,* 103, 5664–5669, doi:10.1073/pnas.0601584103.

Fueglistaler, S., H. Wernli, and T. Peter (2004), Tropical troposphere-to-stratosphere transport inferred from trajectory calculations, *J. Geophys. Res.*, 109, D03108, doi:10.1029/2003JD004069.

Fueglistaler, S., M. Bonazzola, P. H. Haynes, T. Peter (2005), Stratospheric water vapor predicted from the Lagrangian temperature history of air entering the stratosphere in the tropics, *J. Geophys. Res.*, 110 (D8), doi:10.1029/2004JD005516.

Fueglistaler, S., A. E. Dessler, T. J. Dunkerton, I. Folkins, Q. Fu, and P. W. Mote, 2009. Tropical tropopause layer. *Rev. Geophys.,* 47, RG1004.

Gettelman, A., W. J. Randel, F. Wu, and S. T. Massie (2002), Transport of water vapor in the tropical tropopause layer, *Geophys. Res. Lett.*, 29(1), 1009, doi:10.1029/2001GL013818.

Gettelman, A., D. E. Kinnison, T. J. Dunkerton, and G. P. Brasseur (2004), Impact of monsoon circulations on the upper troposphere and lower stratosphere, *J. Geophys. Res.,* 109, D22101, doi:10.1029/2004JD004878.

Harries, J. E. (1976), The distribution of water vapor in the stratosphere, *Rev. Geophys.*, 14(4), 565–575, doi:10.1029/RG014i004p00565.

Harries, J. E., J. M. Russell III, A. F. Tuck, L. L. Gordley, P. Purcell, K. Stone, R. M. Bevilacqua, M. Gunson, G. Nedoluha, and W. A. Traub (1996), Validation of measurements of water vapor from the Halogen Occultation Experiment (HALOE), *J. Geophys. Res.*, 101(D6), 10,205–10,216, doi:10.1029/95JD02933.

Hatsushika, H., and K. Yamazaki (2001), Interannual variations of temperature and vertical motion at the tropical tropopause associated with ENSO, *Geophys. Res. Lett.*, 28(15), 2891–2894, doi:10.1029/2001GL012977.

Highwood, E. J. and Hoskins, B. J. (1998), The tropical tropopause, *Q. J. R. Meteor. Soc.*, 124, 1579–1604, doi:10.1002/qj.49712454911.

Holton, J. R., P. H. Haynes, M. E. McIntyre, A. R. Douglass, R. B. Rood, and L. Pfister (1995), Stratosphere-troposphere exchange, *Rev. Geophys.*, 33(4), 403–439, doi:10.1029/95RG02097.

Holton, J. R., and A. Gettelman (2001), Horizontal transport and the dehydration of the stratosphere, *Geophys. Res. Lett.*, 28(14), 2799–2802, doi:10.1029/2001GL013148.

Jensen, E. J., O. B. Toon, L. Pfister, and H. B. Selkirk (1996), Dehydration of the upper troposphere and lower stratosphere by subvisible cirrus clouds near the tropical tropopause, *Geophys. Res. Lett.*, 23(8), 825–828, doi:10.1029/96GL00722.

Jensen, E., and L. Pfister (2004), Transport and freeze-drying in the tropical tropopause layer, *J. Geophys. Res.*, 109, D02207, doi:10.1029/2003JD004022.

Jones, R. L., Pyle, J. A., Harries, J. E., Zavody, A. M., Russell, J. M. and Gille, J. C. (1986), The water vapour budget of the stratosphere studied using LIMS and SAMS satellite data. *Q. J. R. Meteor. Soc.*, 112. 1127–1143. doi:10.1002/qj.49711247412

Kley, D., E.J. Stone, W.R. Henderson, J.W. Drummond, W.J. Harrop, A.L. Schmeltekopf, T.L. Thompson, R.H. Winkler, 1979: In Situ Measurements of the Mixing Ratio of Water Vapor in the Stratosphere. *J. Atmos. Sci.*, **36**, 2513–2524.

Kuang, Z., G. C. Toon, P. O. Wennberg, and Y. L. Yung (2003), Measured HDO/H_2O ratios across the tropical tropopause, *Geophys. Res. Lett.*, 30(7), 1372, doi:10.1029/2003GL017023.

Lambert, A., W. G. Read, N. J. Livesey, M. L. Santee, G. L. Manney, et al. (2007), Validation of the Aura Microwave Limb Sounder middle atmosphere water vapor and nitrous oxide measurements, *J. Geophys. Res.*, 112, D24S36, doi:10.1029/2007JD008724.

Liu, Y. S., S. Fueglistaler, and P. H. Haynes (2010), Advection-condensation paradigm for stratospheric water vapor, *J. Geophys. Res.*, 115, D24307, doi:10.1029/2010JD014352.

Livesey, N. J., W. G. Read, A. Lambert, R. E. Cofield, D. T. Cuddy, et al. (2007), EOS Aura Microwave Limb Sounder version 2.2 level 2 data quality and description document, *Tech. Rep. JPL D-33509*, 115 pp., Jet Propul. Lab., Pasadena, Calif.

Mastenbrook, H. J. (1971), The variability of water vapor in the stratosphere. *J. Atmos. Sci.*, 28, 1495–1501. doi:10.1175/1520-0469(1971)028<1495:TVOWVI>2.0.CO;2

Mote, P. W., K. H. Rosenlof, J. R. Holton, R. S. Harwood, and J. W. Waters (1995), Seasonal variations of water vapor in the tropical lower stratosphere, *Geophys. Res. Lett.*, 22(9), 1093–1096, doi:10.1029/95GL01234.

Mote, P. W., K. H. Rosenlof, M. E. Mclntyre, E. S. Carr, J. C. Gille, J. R. Holton, J. S. Kinnersley, H. C. Pumphrey, J. M. Russell III, and J. W. Waters (1996), An atmospheric tape recorder: The imprint of tropical tropopause temperatures on stratospheric water vapor, *J. Geophys. Res.*, 101(D2), 3989–4006, doi:10.1029/95JD03422.

Moyer, E. J., F. W. Irion, Y. L. Yung, and M. R. Gunson (1996), ATMOS stratospheric deuterated water and implications for troposphere-stratosphere transport, *Geophys. Res. Lett.*, 23(17), 2385–2388, doi:10.1029/96GL01489.

Murphy, D. M. and Koop, T. (2005), Review of the vapour pressures of ice and supercooled water for atmospheric applications. *Q. J. R. Meteor. Soc.*, 131, 1539–1565. doi: 10.1256/qj.04.94.

Newell, R. E., S. Gould-Stewart (1981), A Stratospheric Fountain?, *J. Atmos. Sci.*, 38, 2789–2796.

Park, M., W. J. Randel, A. Gettelman, S. T. Massie, and J. H. Jiang (2007), Transport above the Asian summer monsoon anticyclone inferred from Aura Microwave Limb Sounder tracers, *J. Geophys. Res.*, 112, D16309, doi:10.1029/2006JD008294.

Pommrich, R., R. Müller, J.-U. Grooß, G. Günther, P. Konopka, M. Riese, A. Heil, M. Schultz, H.-C. Pumphrey, and K. A. Walker, 2010: What causes the irregular cycle of the atmospheric tape recorder signal in HCN? *Geophys. Res. Letters,* **37,** L16805

Potter, B. E. and J. R. Holton (1995), The role of monsoon convection in the dehydration of the lower stratosphere, *J. Atmos. Sci.,* 52, 1034–1050

Randel, W. J., F. Wu, A. Gettelman, J. M. Russell III, J. M. Zawodny, and S. J. Oltmans (2001), Seasonal variation of water vapor in the lower stratosphere observed in Halogen Occultation Experiment data, *J. Geophys. Res.*, 106, 14,313–14,325, doi:10.1029/2001JD900048.

Randel, W. J., F. Wu, and W. Rivera Ríos (2003), Thermal variability of the tropical tropopause region derived from GPS/MET observations, *J. Geophys. Res.*, 108(D1), 4024, doi:10.1029/2002JD002595.

Randel, W. J., F. Wu, S. J. Oltmans, K. Rosenlof, and G. E. Nedoluha (2004), Interannual changes of stratospheric water vapor and correlations with tropical tropopause temperatures. *J. Atmos. Sci.*, 61, 2133–2148, doi:10.1175/1520-0469(2004)061<2133:ICOSWV>2.0.CO;2

Randel, W. J., M. Park, F. Wu, and N. Livesey (2007), A large annual cycle in ozone above the tropical tropopause linked to the Brewer–Dobson circulation. *J. Atmos. Sci.*, 64, 4479–4488, doi:10.1175/2007JAS2409.1.

Randel, W. J., M. Park, L. Emmons, D. Kinnison, P. Bernath, K. A. Walker, C. Boone, and H. Pumphrey (2010), Asian monsoon transport of pollution to the stratosphere, *Science,* 328, 611–613, doi:10.1126/science.1182274

Read, W. G., et al. (2007), Aura Microwave Limb Sounder upper tropospheric and lower stratospheric H_2O and relative humidity with respect to ice validation, *J. Geophys. Res.*, 112, D24S35, doi:10.1029/2007JD008752.

Reid, G. C., and K. S. Gage (1996), The tropical tropopause over the western Pacific: Wave driving, convection, and the annual cycle, *J. Geophys. Res.*, 101(D16), 21,233–21,241, doi:10.1029/96JD01622.

Rienecker, Michele M., et al. (2011), MERRA: NASA's Modern-Era Retrospective Analysis for Research and Applications. *J. Climate*, 24, 3624–3648, doi:10.1175/JCLI-D-11-00015.1

Rind, D., and P. Lonergan (1995), Modeled impacts of stratospheric ozone and water vapor perturbations with implications for high-speed civil transport aircraft, *J. Geophys. Res.*, 100(D4), 7381–7396, doi:10.1029/95JD00196.

Robinson, G. D. (1980), The transport of minor atmospheric constituents between troposphere and stratosphere, *Q. J. R. Meteor. Soc.*, 106, 227–253.

Rosenlof, K. H. (2003), How water enters the stratosphere, *Science*, 302, 1691–1692, doi:10.1126/science.1092703

Scaife, A. A., J. Austin, N. Butchart, S. Pawson, M. Keil, J. Nash, and I. N. James (2000), Seasonal and interannual variability of the stratosphere diagnosed from UKMO TOVS analyses, *Q. J. R. Meteor. Soc.,* 126, 2585–2604, doi:10.1002/qj.49712656812

Schoeberl, M. R., B. N. Duncan, A. R. Douglass, J. Waters, N. Livesey, W. Read, and M. Filipiak (2006), The carbon monoxide tape recorder, *Geophys. Res. Lett.*, 33, L12811, doi:10.1029/2006GL026178.

Schoeberl, M. R., and Dessler, A. E. (2011), Dehydration of the stratosphere, *Atmos. Chem. Phys.,* 11, 8433-8446, doi:10.5194/acp-11-8433-2011.

Sherwood, S. C. (2000), A stratospheric "drain" over the maritime continent, *Geophys. Res. Lett.*, 27(5), 677–680, doi:10.1029/1999GL010868.

Sherwood, S. C., and A. E. Dessler (2000), On the control of stratospheric humidity, *Geophys. Res. Lett.*, 27(16), 2513–2516, doi:10.1029/2000GL011438.

Sherwood, S. C., and A. E. Dessler (2001), A model for transport across the tropical tropopause, *J. Atmos. Sci.*, 58, 765–779, doi:10.1175/1520-0469(2001)058<0765:AMFTAT>2.0.CO;2

Simmons, A. J., Untch, A., Jakob, C., Kållberg, P. and Undén, P. (1999), Stratospheric water vapour and tropical tropopause temperatures in ECMWF analyses and

multi-year simulations, *Q. J. R. Meteor. Soc.*, 125, 353–386. doi:10.1002/qj.49712555318

Solomon, S., K. H. Rosenlof, R. W. Portmann, J. S. Daniel, S. M. Davis, T. J. Sanford, and G. K. Plattner (2010), Contributions of stratospheric water vapor to decadal changes in the rate of global warming, *Science*, 327**,** 1219–1223, doi:10.1126/science.1182488

Thompson, D. W. J., and J. M. Wallace (2000), Annular Modes in the Extratropical Circulation. Part I: Month-to-Month Variability. *J. Climate*, 13, 1000–1016, doi:10.1175/1520-0442(2000)013<1000:AMITEC>2.0.CO;2

Vömel, H., M. Fujiwara, M. Shiotani, F. Hasebe, and S. J. Oltmans (2002), Balloon-borne observations of water vapor and ozone in the tropical upper troposphere and lower stratosphere, *J. Geophys. Res.*, 107(D14), 4210, doi:10.1029/2001JD000707.

Wang, B., and LinHo (2002), Rainy season of the Asian-Pacific summer monsoon, *J. Climate,* 15, 386–398, doi:10.1175/1520-0442(2002)015<0386:RSOTAP>2.0.CO;2

Wright, J. S., R. Fu, S. Fueglistaler, Y. S. Liu, and Y. Zhang (2011), The influence of summertime convection over Southeast Asia on water vapor in the tropical stratosphere, *J. Geophys. Res.*, 116, D12302, doi:10.1029/2010JD015416.

APPENDIX A

TABLES

Table 1: Comparison of monthly means and annual statistics of the model H_2O concentration including and excluding FDP events that occurred within 2 days of initialization.

Month	**Model H_2O Including First and Second Day FDP Points**	**Model H_2O Excluding First and Second Day FDP Points**	**Difference**
January	2.77493	2.64040	0.13453
February	2.83543	2.64560	0.18983
March	3.15672	2.91607	0.24065
April	3.40217	3.15878	0.24339
May	3.81406	3.53052	0.28354
June	4.48350	4.13616	0.34734
July	4.88318	4.39982	0.48336
August	5.17143	4.67829	0.49314
September	5.10134	4.61464	0.48670
October	4.50097	4.14531	0.35566
November	3.68960	3.48889	0.20071
December	3.00456	2.85641	0.14815
Mean	3.90149	3.60091	0.30058
Standard Deviation	0.85542	0.73490	0.12601

Table 2: MERRA daily reanalysis monthly mean saturation H_2O concentration for parcels undergoing their FDP event within various distances from the equator.

Month	**Maximum distance from equator**		
	25 degrees	35 degrees	45 degrees
January	2.62035	2.62166	2.64040
February	2.62998	2.63202	2.64560
March	2.90759	2.90825	2.91607
April	3.14892	3.14954	3.15878
May	3.52493	3.52570	3.53052
June	4.13425	4.13626	4.13616
July	4.39005	4.39361	4.39982
August	4.63933	4.64116	4.67829
September	4.55838	4.55904	4.61464
October	4.08502	4.08481	4.14531
November	3.45429	3.45561	3.48889
December	2.83126	2.83191	2.85641

Table 3: Count of FDP events occurring within each month and meteorological season overall and within various altitude ranges.

Month	**FDP Event Count**	<70 hPa	70-80 hPa	80-90 hPa	90-100 hPa	100-110 hPa	>110 hPa
January	136,148	2,772	26,006	63,959	39,327	4,081	3
February	106,563	1,008	13,993	43,408	40,848	7,277	29
March	101,686	87	3,244	34,688	51,495	12,092	80
April	101,853	26	1,703	33,517	51,541	14,927	139
May	109,432	1	1,201	26,500	54,065	27,267	398
June	120,755	1	175	12,452	60,241	46,280	1,606
July	94,915	0	45	5,627	44,787	41,808	2,648
August	72,799	0	10	1,347	33,657	35,731	2,054
September	64,339	0	138	7,382	32,882	23,471	466
October	95,571	8	2,143	35,244	45,511	12,637	28
November	123,325	423	15,056	70,563	33,967	3,312	4
December	213,582	2,309	37,435	81,845	32,317	2,331	4
DJF	398,952	6,089	72,434	189,212	112,492	13,689	36
MAM	312,971	114	6,148	94,705	157,101	54,286	617
JJA	288,469	1	230	19,426	138,685	123,819	6,308
SON	283,235	431	17,337	113,189	112,360	39,420	498
Total	1,283,627	6,635	101,149	416,532	520,638	231,214	7,459

Table 4: Same as Table 3, but for latitude ranges.

	30-40°S	**20-30°S**	**10-20°S**	**0-10°S**	**0-10°N**	**10-20°N**	**20-30°N**	**30-40°N**
January	0	1,941	27,800	54,597	38,551	12,746	539	2
Febru-ary	0	1,457	17,442	38,306	36,741	11,935	683	0
March	0	792	14,203	30,711	38,185	16,965	830	0
April	0	600	13,580	29,384	38,870	18,696	723	0
May	0	598	15,991	30,239	39,769	21,911	924	1
June	3	968	22,236	30,044	38,747	26,370	1,787	4
July	0	1,134	25,867	24,735	23,780	16,599	2,791	8
August	0	696	21,044	18,340	18,039	9,696	2,697	6
Septem-ber	0	1,005	23,019	21,170	12,022	6,015	1,107	1
October	1	1,744	31,188	35,344	18,249	7,838	1,202	5
Novem-ber	0	924	28,445	55,361	28,268	9,743	583	1
Decem-ber	0	999	33,116	68,115	39,921	13,327	767	3
DJF	0	4,397	78,358	161,018	115,213	38,008	1,989	5
MAM	0	1,990	43,774	90,334	116,824	57,572	2,477	1
JJA	3	2,798	69,147	73,119	80,566	52,665	7,275	18
SON	1	3,673	82,652	111,875	58,539	23,596	2,892	7
Total	4	12,858	273,931	436,346	371,142	171,841	14,633	31

APPENDIX B

FIGURES

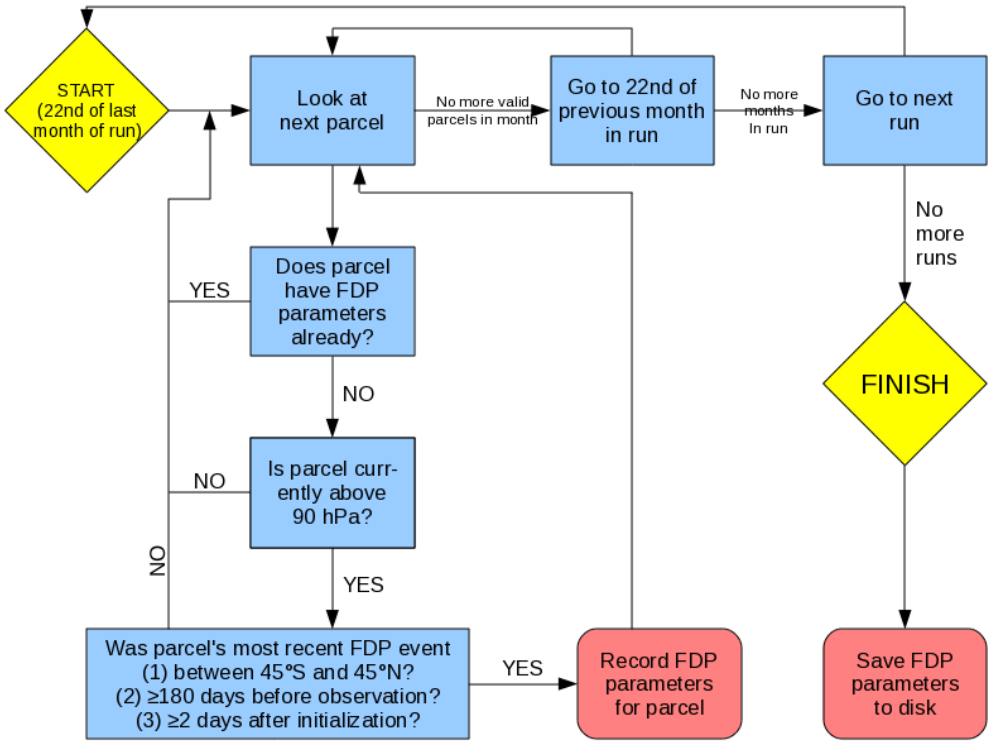

Figure 1: Flowchart depicting the FDP point determination process.

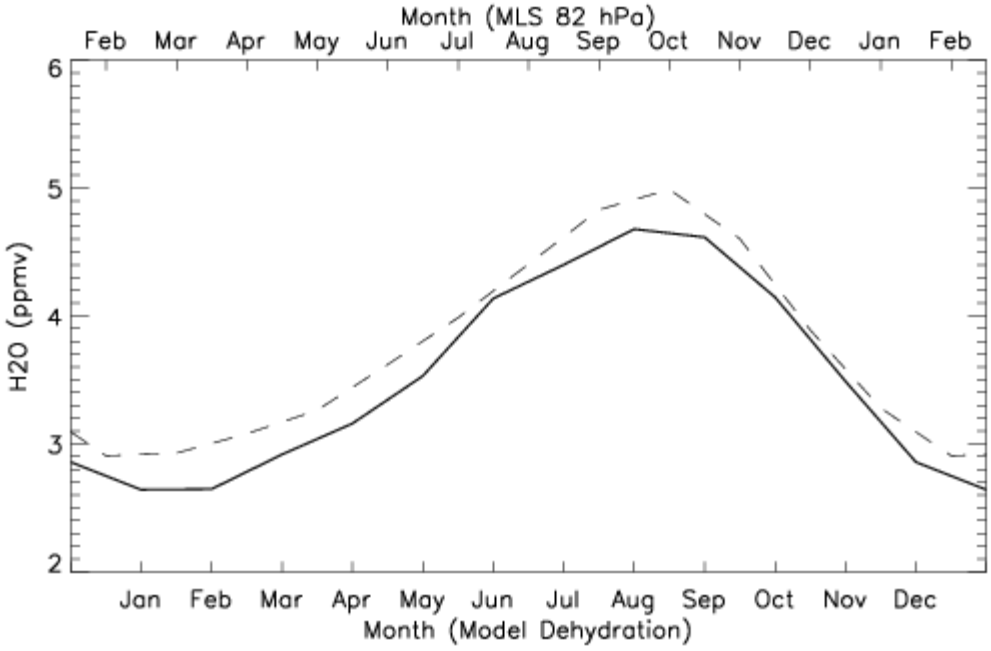

Figure 2: Model-produced mean final parcel saturation water vapor concentration (1993-2010) as a function of month of final dehydration (solid line, bottom axis); monthly mean MLS measured water vapor concentration at 82 hPa lagged by 1.5 months (dashed line, top axis).

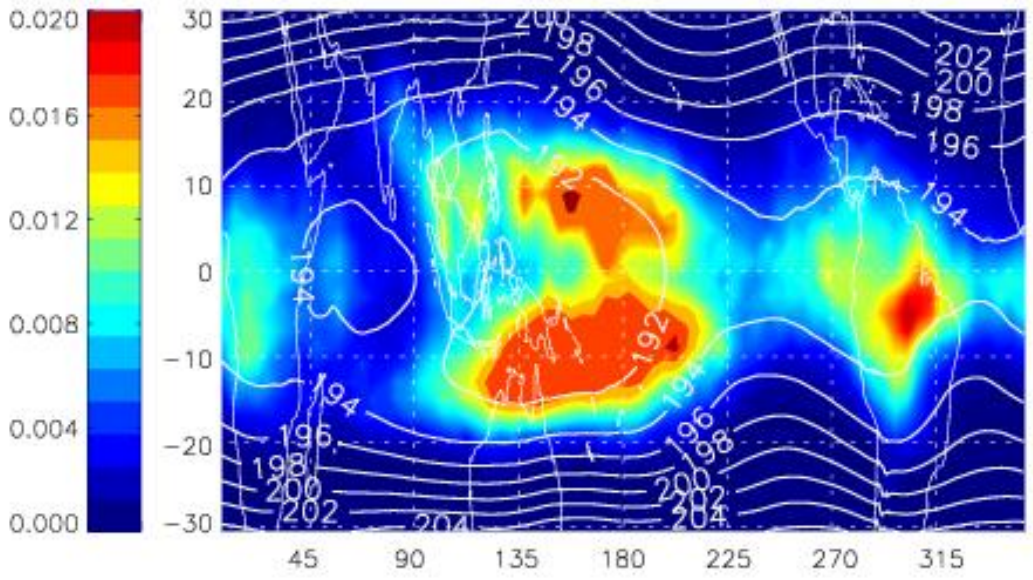

Figure 3: Latitude-longitude frequency of FDP events (percent per degree latitude per degree longitude) during 1993-2010 (colored), with MERRA reanalysis 100 hPa temperature contoured.

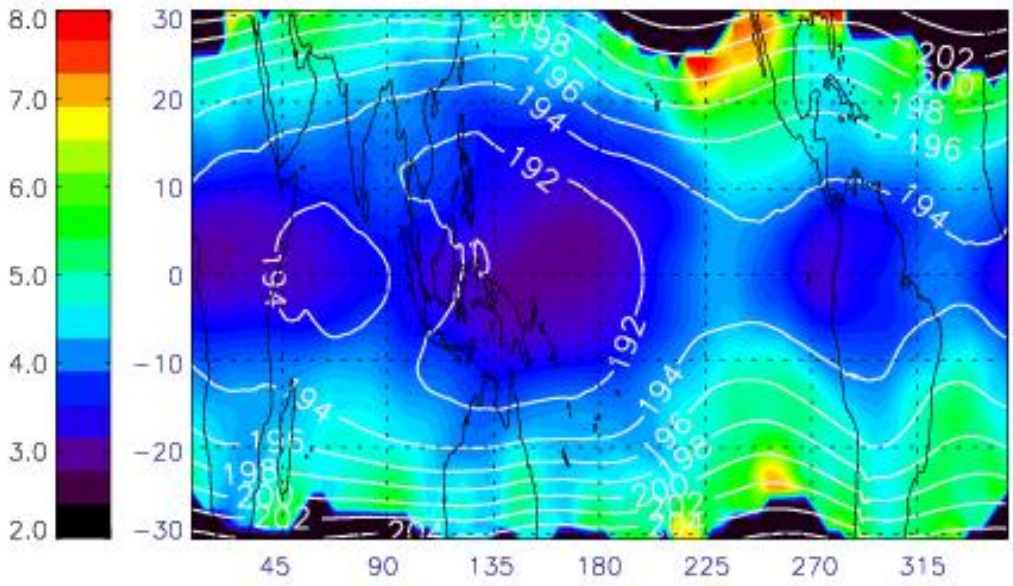

Figure 4: Mean final saturation water vapor concentration (ppmv) as function of latitude and longitude (1993-2010, colored), with MERRA reanalysis 100 hPa temperature (contoured)

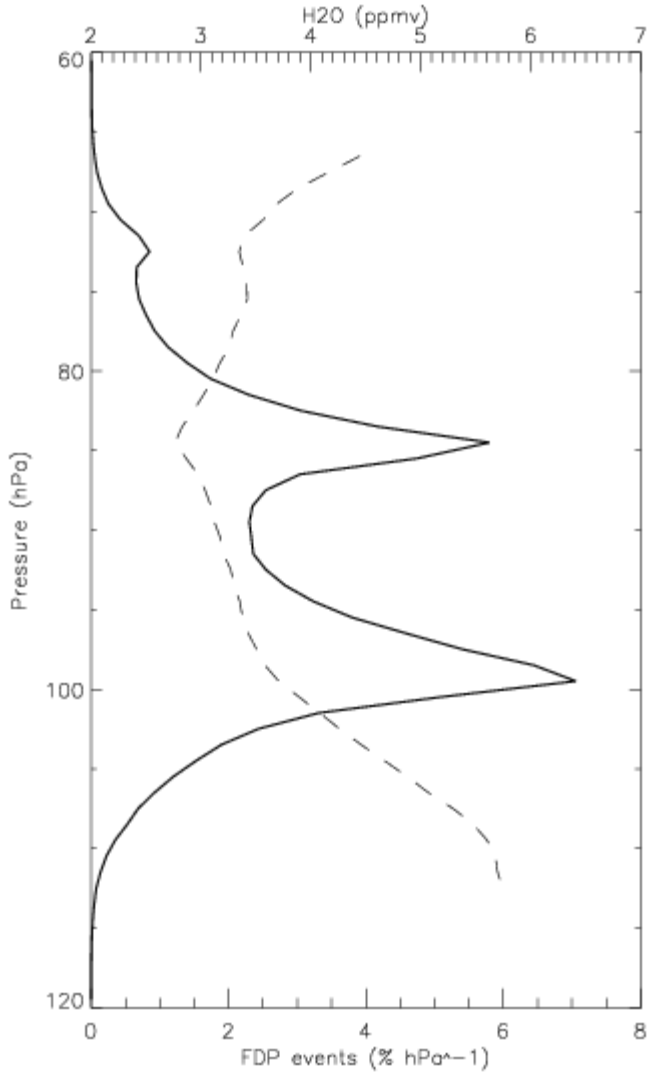

Figure 5: Vertical frequency of FDP events (percent hPa^{-1}), solid line, bottom axis); mean final saturation water vapor concentration (ppmv) as function of pressure (dashed line, top axis).

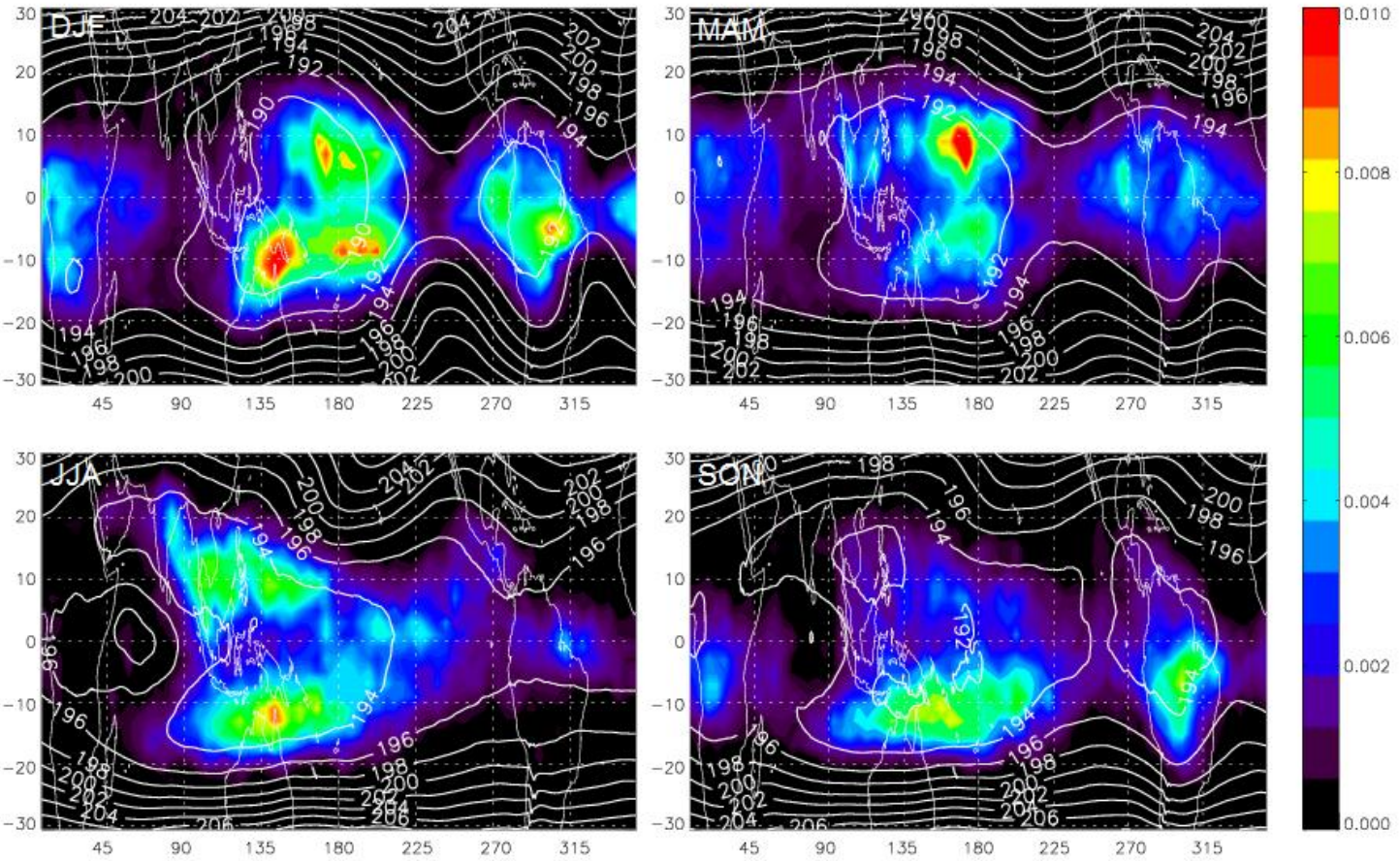

Figure 6: Latitude-longitude frequency of FDP events (percent per degree latitude per degree longitude) during December–February (upper left), March–May (upper right), June–August (lower left), September–November (lower right) 1993–2010 (colored). The sum of the panels equals Figure 3. Contours are the MERRA reanalysis average 100 hPa temperature for the season.

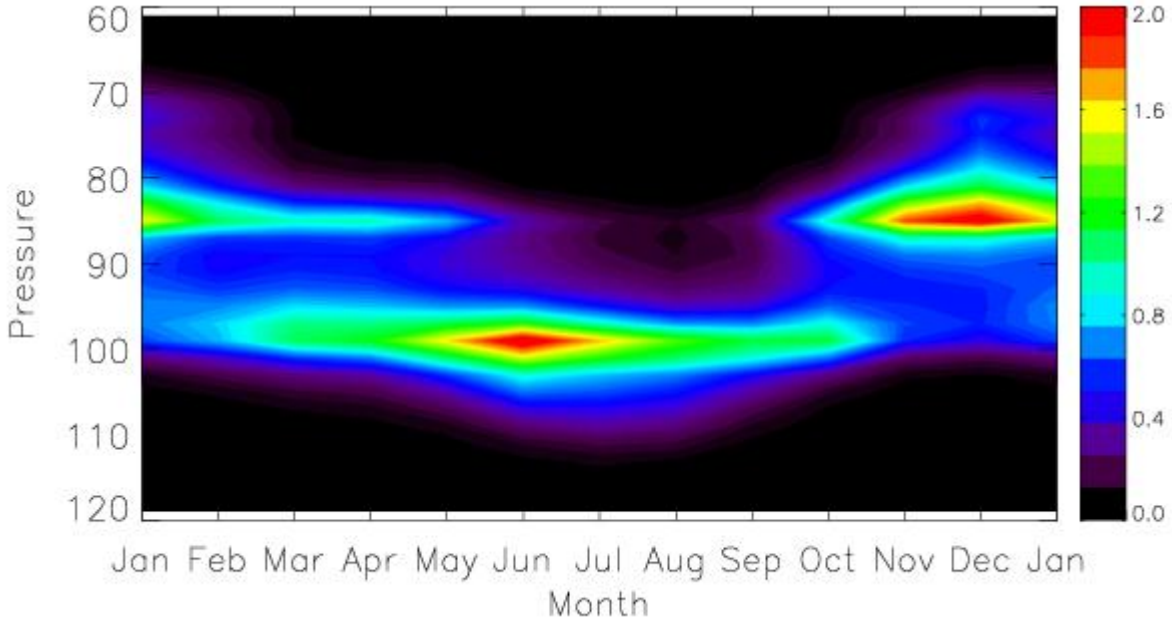

Figure 7: Vertical frequency of FDP events (percent per hectopascal) as a function of month of FDP event (abscissa) and pressure of FDP event (ordinate).

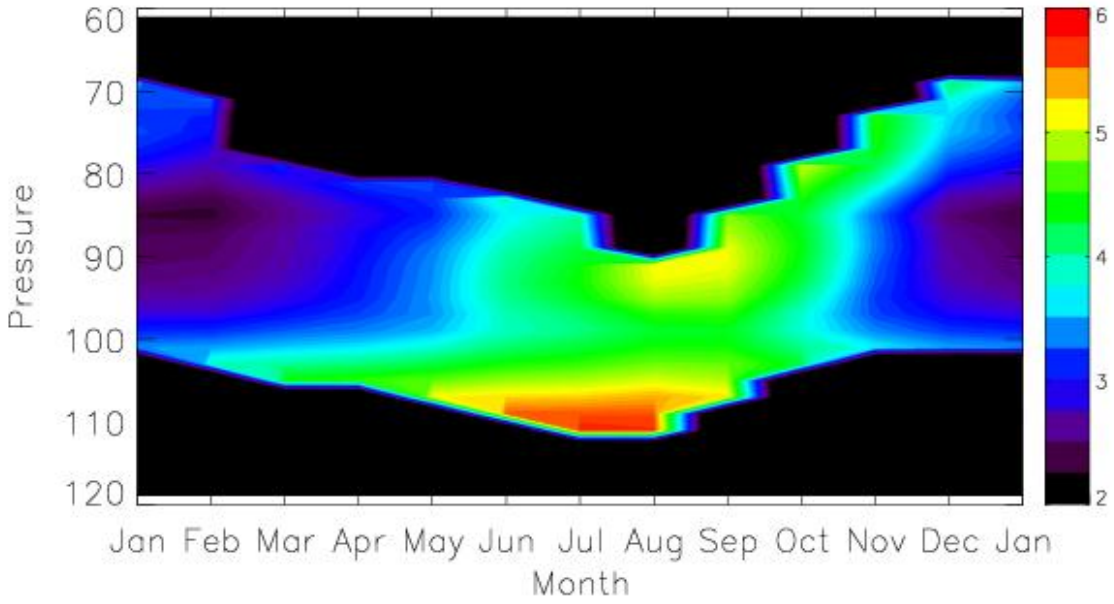

Figure 8: Mean final saturation water vapor concentration (ppmv) as a function of month of FDP event (abscissa) and pressure of FDP event (ordinate).

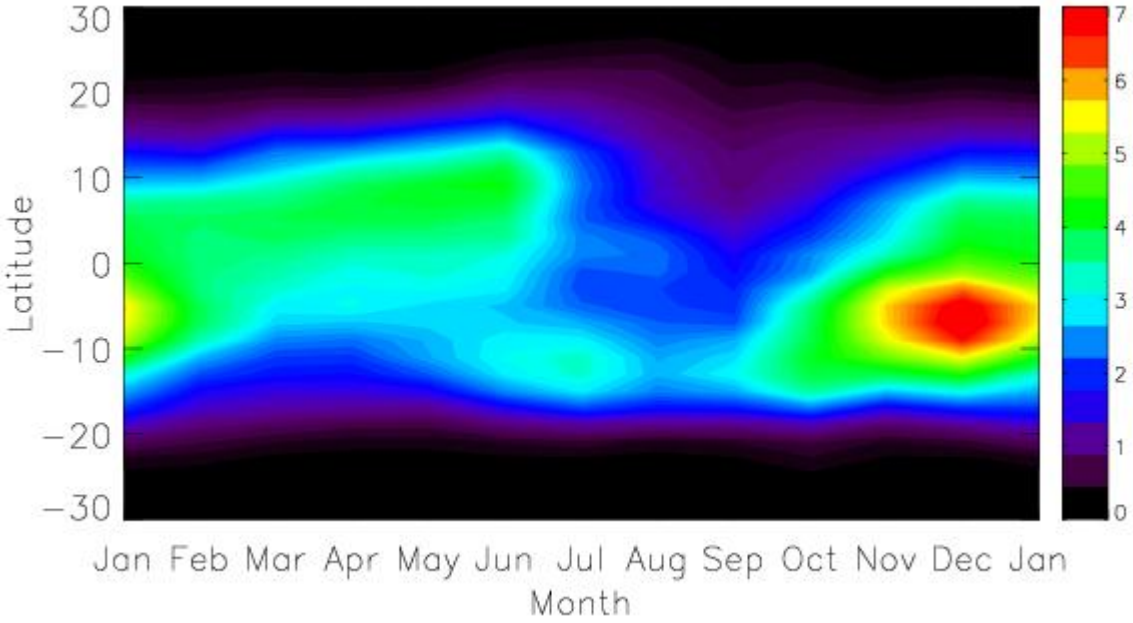

Figure 9: Zonal frequency of FDP events (percent per degree latitude) as a function of month of FDP event (abscissa) and latitude of FDP event (ordinate).

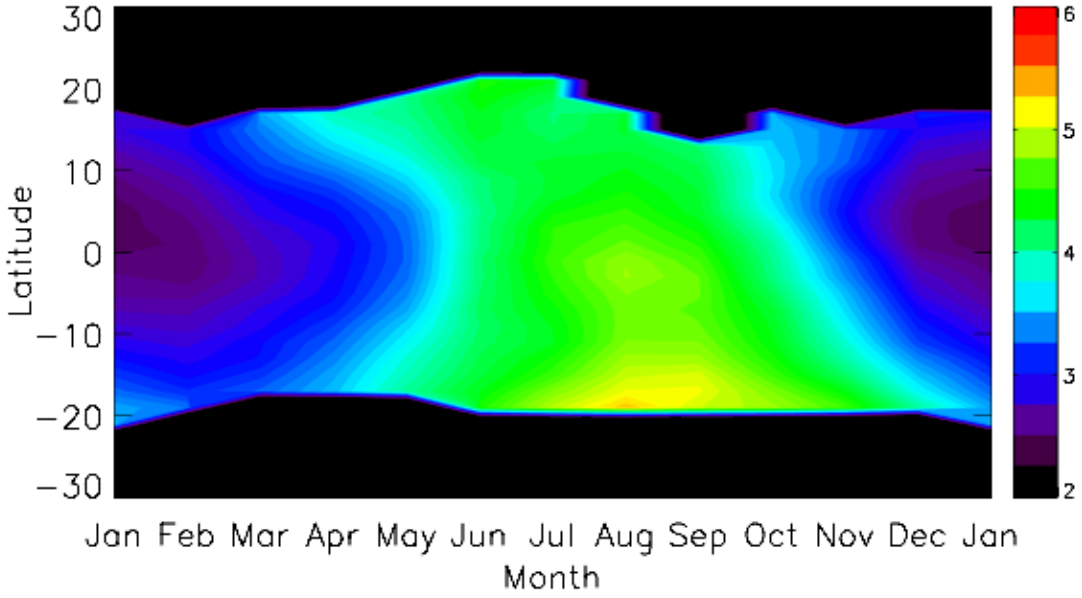

Figure 10: Mean final saturation water vapor concentration (ppmv) as a function of month of FDP event (abscissa) and latitude of FDP event (ordinate).

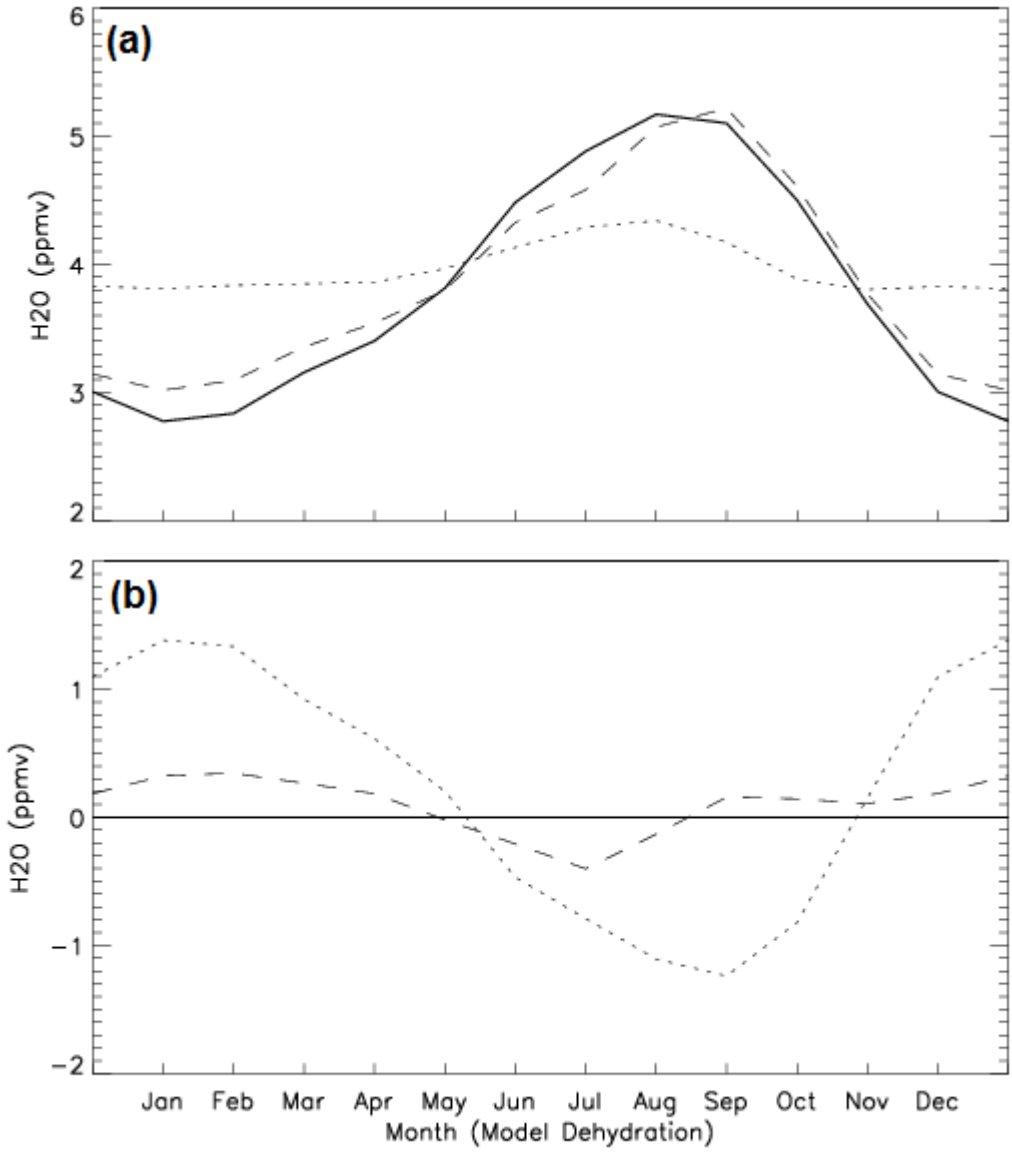

Figure 11: (a) Model-produced mean final parcel saturation water vapor concentration (1993-2010) as a function of month of final dehydration (black); the same, but holding the shape of the vertical profile of parcel dehydration constant (blue); the same, but holding the shape of the vertical profile of final saturation water vapor concentration constant (red). (b) Monthly anomalies of these with respect to the model-produced mean final parcel saturation water vapor concentration.

VITA

Name: Aaron Joseph Christenberry

Address: Eller O&M Building
3148 TAMU
College Station, TX 77843-3148

Email Address: achristenberry@neo.tamu.edu
aaron@christenberry.com

Education: B.S., Meteorology, University of Oklahoma, 2010
M.S., Atmospheric Sciences, Texas A&M University, 2012